

Nitric oxide breath testing by tunable-diode laser absorption spectroscopy: application in monitoring respiratory inflammation

Chad Roller, Khosrow Namjou, James D. Jeffers, Mark Camp, Adam Mock, Patrick J. McCann, and Joe Grego

We used a high-resolution mid-IR tunable-laser absorption spectroscopy (TLAS) system with a single IV–VI laser operating near 5.2 μm to measure the level of exhaled nitric oxide (eNO) in human breath. A method of internal calibration using simultaneous eNO and exhaled CO_2 measurements eliminated the need for system calibration with gas standards. The results observed from internally calibrating the instrument for eNO measurements were compared with measurements of eNO calibrated to gas standards and were found to be similar. Various parameters of the TLAS system for eNO breath testing were examined and include gas cell pressure, exhalation time, and ambient NO concentrations. A reduction in eNO from elevated concentrations (~ 44 parts in 10^9) to near-normal levels (< 20 parts in 10^9) from an asthmatic patient was observed after the patient had received treatment with an inhaled glucocorticoid anti-inflammatory medication. Such measurements can help in evaluating airway inflammation and in monitoring the effectiveness of anti-inflammatory therapies. © 2002 Optical Society of America

OCIS codes: 000.1430, 140.3070, 300.1030, 300.6340.

1. Introduction

There has been much interest in the detection of exhaled nitric oxide (eNO) in medicine for directly assessing airway inflammation. Clinical eNO breath analysis provides the physician a simple and noninvasive window into the activities of disease, including asthma, chronic obstructive pulmonary disorder, and cystic fibrosis, in the lower airways.¹ There have been numerous studies with which eNO was monitored in children and adults that focused mainly on the use of such measurements for assisting in initial investigations for the presence of airway inflammation associated with asthma and monitor-

ing the effectiveness of anti-inflammatory glucocorticoid medications aimed at inhibiting nitric oxide (NO) producing synthase activity.^{2,3} Current diagnostic tests such as spirometry provide limited and only indirect information about the actual degree of inflammation in the lower airways.⁴ It is worth noting that there is a lack of objective and routine clinical diagnostic tests for assessing airway inflammation in children younger than 8 years of age.

Various technologies have been proposed for next-generation medical devices that will be capable of making routine eNO measurements of patients in a clinical setting. Chemiluminescence is the most recently proposed technique for this purpose and has given rise to numerous insightful reports, many of which are referenced in Ref. 5. Based on these reports, the American Thoracic Society has proposed standardized breath-collection procedures and the European Respiratory Society has stated that eNO serves as a valid biological marker of airway inflammation and can be used to evaluate the effectiveness of treatments.^{6,7} However, several factors have hampered the adoption of chemiluminescence in the United States, and these include the need for frequent calibrations and the necessity for the patient to maintain constant exhalation flows.⁸ Although en-

C. Roller, K. Namjou (knamjou@ekipstech.com), and J. D. Jeffers are with Ekips Technologies, Inc., 710 Asp Avenue, Suite 308, Norman, Oklahoma 73069. M. Camp is with The Lung Center, Inc., Norman, Oklahoma 73071. A. Mock is with Department of Electrical and Computer Engineering, Columbia University, New York, New York 10027. P. J. McCann and J. Grego are with School of Electrical and Computer Engineering, University of Oklahoma, Norman, Oklahoma 73019.

Received 21 March 2002; revised manuscript received 20 June 2002.

0003-6935/02/286018-12\$15.00/0

© 2002 Optical Society of America

ogenous and exogenous water vapor, carbon dioxide, and ammonia can contribute to inaccurate eNO measurements with chemiluminescence instruments,⁹ the reasons mentioned above are most likely responsible for the large variations of results reported in various clinical studies.⁵ Because of the complexity of breath collection by chemiluminescence, the technique is not recommended for children younger than 8 years of age. Fourier-transform IR spectroscopy and gas chromatography coupled with mass spectroscopy are selective and sensitive but cannot perform rapid trace-gas measurements, which are desired for clinical use. To date, the U.S. Food and Drug Administration has not approved any medical device for NO breath monitoring, but it has assigned the product code MXA for such a device, and efforts to obtain approval are ongoing.

Mid-IR high-resolution spectroscopy in the 3–20- μm region is an analytical technique that can permit rapid and selective measurements of eNO with the required sensitivity of ~ 1 part in 10^9 (ppb). Tunable laser absorption spectroscopy (TLAS) is a common technique for laboratory and scientific field measurements of trace gases with absorption features residing in the mid-IR region of the electromagnetic spectrum. Two major factors have prevented the practical application of TLAS in clinical settings for routine breath analysis. First, the need for cryogenic cooling of some mid-IR lasers requires a large liquid- N_2 supply, which is not readily available in most clinical settings. Second, the need for frequent calibrations with calibration gases can be burdensome and limits the operators of the instrument to trained personnel. A brief overview of candidate mid-IR spectroscopic gas sensing technologies for eNO breath measurements is now given.

2. Mid-IR Laser Gas Sensing Technologies

Mid-IR sources for TLAS systems that are currently available include quantum cascade (QC) distributed-feedback (DFB) lasers and IV–VI diode lasers. QC lasers can be operated either in continuous-wave (cw) mode at cryogenic temperatures or by pulsing of the pump current with duty cycles that are typically $< 1\%$ at temperatures ranging from -40°C to above room temperature. There is a significant reduction in average optical output power when the QC laser is pulsed, but average optical output powers in the milliwatt range can still be achieved without the need for liquid- N_2 sources. Pulsed QC lasers have demonstrated room-temperature operation, and Namjou *et al.*¹⁰ reported measurements of N_2O in the low parts in 10^6 (ppm) range by pulsing the laser and using second-harmonic ($2f$) detection. NO trace-gas measurements at concentrations of less than 10 ppb with rapid integration times (≤ 5 s) for pulsed QC DFB lasers operated at near room temperature in the 5.1 to 5 μm region can be difficult to achieve. Pulsing the QC laser current can result in laser linewidth broadening caused by frequency chirp reducing the effective sensitivity. However, the frequency chirp effect when QC lasers are pulsed could be minimized

by incorporation of advanced data-acquisition techniques. Research into improving mid-IR QC laser technology is ongoing, and room-temperature cw QC lasers operating at 9.1 μm have recently been demonstrated with maximum optical output powers of 17 mW.¹¹ Extension of this achievement toward fabrication of room-temperature cw QC lasers operating at shorter wavelengths at which NO absorption lines can be measured is a worthwhile objective.

IV–VI diode lasers (also known as lead-salt lasers) have been used to make sensitive measurements of many molecular species. Specifically, cryogenically cooled IV–VI lasers operated in cw mode have been used to measure CO, NO, CO_2 , NH_3 , and CH_4 in the exhaled breath of human subjects.^{12,13} IV–VI lasers with emission wavelengths of 4–8 μm composed of conventional double-heterostructure p–n junctions are commercially available. As with QC lasers, research into improving mid-IR IV–VI laser technology is ongoing. For example, it has been shown¹⁴ that one can achieve a significant increase in operating temperatures by removing the growth substrate from an epitaxially grown laser structure^{15,16} and applying a second heat sink to improve heat dissipation in the active region. Other recent achievements that illustrate the possibility of room-temperature cw laser emission include demonstration of above-room-temperature cw photoluminescence from IV–VI multiple-quantum-well structures^{17–19} and above-room-temperature operation near 4.1 μm of an optically pumped vertical-cavity surface-emitting laser.²⁰ The results of this theoretical and experimental work show that significant improvements in IV–VI laser technology are possible, and commercialization of novel mid-IR IV–VI lasers with improved operating characteristics is a realistic expectation. Further development of IV–VI laser technology, as with QC laser technology, will permit significant reductions in the size and cost of chemical sensing instruments designed for trace-gas measurements and clinical breath analysis.

An alternative to waiting for improvements in the operating temperatures of mid-IR laser sources is to eliminate the need for liquid- N_2 refills by using a closed-cycle cryogenic refrigerator to cool both the mid-IR laser and the mid-IR detector in the TLAS system. That is the method employed and described in the research reported in this paper. With this in mind, the TLAS techniques described here are potentially suitable for either IV–VI or QC lasers.

Of equal importance to the tunable laser in a mid-IR high-resolution spectroscopy system is the choice of gas cell and detection technique. A long optical path length is needed for sensitive measurements, and a small gas-cell volume is needed for fast gas exchange rates and rapid measurements. Cavity ring-down spectroscopy (CRDS) gas cells can achieve optical path lengths of several kilometers and gas cell volumes near $\sim 15\text{ cm}^3$. The CRDS technique measures the decay times of cavity modes and has been used to measure 48.4 ± 0.7 ppb NO in pure N_2 with integration times of ~ 8 s.²¹ In the study

described in Ref. 21, CRDS with cw QC lasers was not able to observe eNO in breath near 1921.6 cm^{-1} because of strong interference from CO_2 absorption lines nearby at 1921.575 and 1921.641 cm^{-1} , which has high concentrations in breath of approximately 4% CO_2 . NO absorption lines located near 1900 cm^{-1} , where there is a larger separation between NO and CO_2 absorption features,²¹ may be better candidates for breath analysis applications that use CRDS. Herein, all techniques other than CRDS that are discussed are based on intensity measurements, whereas CRDS is based on cavity decay times and is independent of laser optical output power fluctuations.

Cavity enhanced spectroscopy takes advantage of low-loss dielectric mirrors in the IR and can achieve optical path lengths up to ~ 1 km and cell volumes below 20 cm^3 . A 670-m optical path-length cavity enhanced spectroscopy gas cell has been used with quasi-cw QC lasers (duty cycle, $\sim 50\%$) at cryogenic temperatures to measure NO, but it was not able to achieve the required sensitivities for measurements of eNO in human breath.²² In the same cryogenically cooled quasi-cw QC laser system, the cavity enhanced spectroscopy cell was replaced with a multipass Herriott cell of 100-m optical path length and 3.5-L cell volume. This system was capable of measuring eNO in human breath. The minimum detectable limits for the cryogenically cooled QC laser system coupled with a Herriott cell were reported to be ~ 2.6 ppb, with a measurement integration time of 200 s.²²

TLAS systems equipped with IV–VI lasers in conjunction with either a Herriott or a multipass White cell have been used in studies that measured eNO in human breath.^{23,24} IV–VI lasers have suitable characteristics for breath analysis, such as sufficient single-mode powers (~ 500 μW), narrow spectral linewidths (~ 100 MHz),^{25,26} and wide tunability (~ 200 cm^{-1} with temperature tuning and ~ 3 cm^{-1} with injection current tuning). These characteristics give TLAS instruments with IV–VI lasers high sensitivities, high molecular selectivity, rapid response times, and the ability to measure multiple trace gases simultaneously. Until QC lasers demonstrate sensitive and near real-time measurements of eNO at thermoelectrically cooled or higher laser operating temperatures, IV–VI lasers will be the most attractive and cost-effective mid-IR tunable diode lasers to use for breath analysis, especially when cryogenic temperatures are unavoidable (see Table 1). The narrow linewidths of IV–VI lasers allow measurements of CO_2 and NO to be made simultaneously in the region near 1912.8 cm^{-1} . Because optical output powers from IV–VI lasers can vary over time, CO_2 can be used to normalize absorption magnitudes and calculate eNO concentrations without the need for calibration procedures that use calibration gases or added optics to measure reference spectra.

It is useful to compare TLAS systems equipped with QC lasers and IV–VI lasers designed for performing eNO measurements in adults. The cryo-

Table 1. eNO Measurements of QC DFB and IV–VI Lasers

Measured Property	IV–VI Laser ^a	QC DFB Laser ^b
Measured NO line wavelength	1850.2 cm^{-1}	1918.7 cm^{-1}
NO line intensity ($\text{cm}^{-1}/\text{molecule cm}^{-2}$)	1.03×10^{-19}	8.09×10^{-21}
Optical output power	Not reported ^c	80 mW
Sensitivity	~ 1 ppb	~ 2.6 ppb
Operating temperature	110 K	< 120 K
Optical path length	8 m	100 m
Integration time	0.5 s	200 s
Number of spectral coverages	64	10,000
Near real-time analysis	Yes	No
Typical power dissipation (not reported)	< 1 W ^d	> 5 W ^e

^aRef. 24.

^bRef. 22.

^cTypical maximum optical output powers for IV–VI lasers are < 2 mW.

^dPower dissipation of less than 5 W is required for the cryogenic cooling system described in this paper. Excessive heat dissipation prevented high-power measurements of cw QC lasers with a Janis closed-cycle He cryostat in the research reported in Ref. 27.

^eRef. 28.

genically cooled TLAS system with a cw QC laser described in Ref. 22 incorporated a 100-m optical path-length Herriott cell and achieved an estimated minimum detection limit for NO of ~ 2.6 ppb for a 200-s integration time. The TLAS system equipped with a cw IV–VI laser with an 8-m optical path-length Herriott cell as described in Ref. 24 achieved an estimated similar minimum detection limit of ~ 1 ppb with an ~ 0.5 -s integration time. Table 1 compares the operational characteristics of the two systems. The most noticeable difference between the QC laser system and the IV–VI laser system is the much shorter integration time for the IV–VI laser system, which is sufficiently short to permit real-time measurements of eNO during an exhalation. Breath analysis with long integration times is possible when off-line techniques are used, and chemiluminescence experiments comparing on-line (real-time) and off-line eNO measurements have suggested that either technique is suitable.¹ However, real-time measurements have the distinct advantage of giving instant feedback for verification of correct breath donations.

To reach cryogenic temperatures, TLAS systems that use IV–VI lasers generally require liquid N_2 , which results in the need for frequent refills and an available liquid- N_2 source. Replacing liquid- N_2 Dewars with a closed-cycle cryogenic refrigerator capable of continuous operation eliminates the need for liquid- N_2 refills and allows for long periods of convenient operation. Modern closed-cycle refrigerators can achieve continuous maintenance-free operation over a 5-year period, a more than adequate operational time for successful deployment in a clinical setting.

In this paper we describe a liquid- N_2 -free TLAS system equipped with a IV–VI laser operating near

5.2 μm for the purpose of analyzing eNO and exhaled CO_2 (e CO_2) simultaneously in expired breath. The system required no consumables other than disposable mouthpieces for breath analysis. Absorption measurements were performed with a 107-m multipass White cell with a 16-L volume. A closed-cycle cryogenic refrigerator was used to maintain cryogenic laser operating temperatures below 120 K. These refrigerators can dissipate ~ 5 W of power at typical laser heat-sink temperatures of ~ 90 K. IV–VI lasers are well suited for cooling with such a system because they typically generate less than 1 W of waste heat. By contrast, QC lasers with their large compliance voltages often generate more than 10 W of waste heat.^{27,28} The system further takes advantage of the ability of a single IV–VI laser to measure H_2O , CO_2 , and NO simultaneously, which eliminates the need for calibration gases, reference cells, and reference detectors.²³ A breath-collection apparatus was fabricated to collect and sample breath in close accordance to the recommendations suggested by the American Thoracic Society. Daily breath measurements from five human volunteers over a period of 10 working days were performed. Daily eNO concentrations measured from these five individuals calculated with e CO_2 end-tidal absorption magnitudes as a reference were compared with concentrations obtained by comparison with a calibrated NO gas standard. The effect of elevated NO levels in the ambient air on calculated eNO concentrations when e CO_2 was used as an internal reference was also studied. To test the flexibility of the internal calibration scheme and to simulate measurements of a child's breath, we performed experiments in which an adult's breath was measured at different exhalation times from 5 to 20 s. Finally, suggestions for future research to establish better-standardized methodologies for implementing internal calibration for eNO by use of e CO_2 are given.

3. Spectroscopic Considerations for H_2O , CO_2 and NO near 5.2 μm

A brief discussion of specific absorption-line attributes for the molecules of interest (NO, CO_2 , and H_2O) from 1912.5 to 1913.0 cm^{-1} is given. The $R(10.5)$ NO lines located at 1912.7937–1912.7956 cm^{-1} have a maximum intensity of $1.032 \times 10^{-20} \text{ cm}^{-1}/(\text{molecule cm}^{-2})$ and are separated by 0.05 cm^{-1} from the nearest H_2O and CO_2 absorption lines. The single CO_2 absorption line [$P(6)$ at 1912.96 cm^{-1}] was measured and has a modest intensity greater than $1.134 \times 10^{-25} \text{ cm}^{-1}/(\text{molecule cm}^{-2})$. There is a second measurable CO_2 line, located at 1912.69 cm^{-1} , with an intensity of $1.009 \times 10^{-26} \text{ cm}^{-1}/(\text{molecule cm}^{-2})$. Also measured simultaneously with CO_2 and NO was H_2O , which has a strong absorption line located at 1912.5 cm^{-1} with an intensity of $1.110 \times 10^{-23} \text{ cm}^{-1}/(\text{molecule cm}^{-2})$. This unambiguous absorption feature is visible in exhaled breath and in ambient air. The region near 5.2 μm contains adequate separation of NO, CO_2 , and H_2O lines, mainly as a result of the narrow line widths of

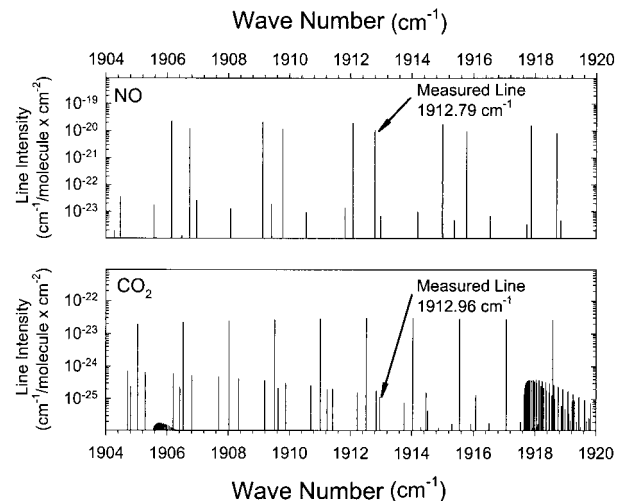


Fig. 1. NO and CO_2 line intensities in the region near 5.2 μm of the IR spectrum. Data are from the HITRAN '96 database.²⁸

IV–VI lasers. The NO and CO_2 absorption lines of interest from 1904 to 1920 cm^{-1} obtained from the HITRAN database²⁹ are shown in Fig. 1. There are other possible candidate NO and CO_2 absorption lines for simultaneous measurements without interference from each other at 1895–1925 cm^{-1} , which are adequate for the eNO breath analysis procedure as described in this paper.

4. Experimental Design and Breath Collection Apparatus

The TLAS system design is shown in Fig. 2. A single IV–VI laser (Ekips Technologies, Norman, Okla.) with typical optical output power of 300 μW was mounted onto a temperature-controlled stage inside a sealed cryostat kept at cryogenic temperatures with a closed-cycle cryogenic refrigerator rated for continuous maintenance-free operation (CryoTiger from APD Cryogenics, Allentown, Pa.). The beam emit-

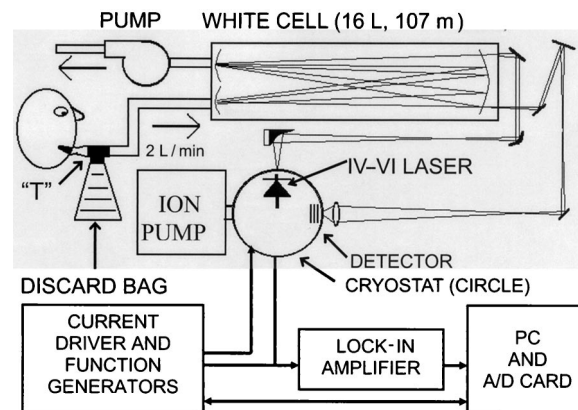


Fig. 2. Schematic of the breath-collection apparatus and the TLAS system equipped with a IV–VI mid-IR laser. The sealed cryostat under vacuum houses the IV–VI laser and the mid-IR detector. Two mass-flow controllers in a parallel configuration (not shown) maintain a constant flow of 2 L/min through the White cell.

ted from the IV–VI laser was directed first through a ZnSe window and onto an off-axis parabolic mirror to collimate the beam. A combination of flat and concave mirrors was used to direct the beam through a 107-m multipass White cell (Infrared Analysis, Anaheim, Calif.). On exiting the White cell, the beam was focused with a ZnSe lens and passed through a ZnSe window onto a HgCdTe mid-IR photovoltaic detector also located inside the cryostat. An integrated heater and temperature controller (Lakeshore, Westerville, Ohio) maintained stable laser operating temperatures at 102 K with an accuracy of ± 0.01 K.

A low-noise laser current driver supplied currents from 800 to 900 mA. A sawtoothed voltage ramp of 40 Hz and $0.11 V_{pp}$ (where pp is peak to peak) was used to tune the single-mode laser emission from 1912.5 to 1913.0 cm^{-1} . Superimposed onto the sawtooth ramp was a smaller triangle waveform at 26.5 kHz and $0.01 V_{pp}$ to modulate the laser emission frequency. The output of the photovoltaic detector was preamplified before a commercial lock-in amplifier (Stanford Research Systems, Sunnyvale, Calif.) sampled the signal at twice the modulation frequency, a procedure known as second-harmonic ($2f$) detection. A transistor–transistor logic signal from the 40-Hz ramp waveform generator was used to trigger the analog-to-digital (A/D) acquisitions of the output signal from the lock-in amplifier. A personal computer (PC) controlled a 12-bit analog-to-digital converter card (National Instruments, Austin, Tex.) and acquired 500 data points per scan at a sampling frequency of 20 kHz. To reduce high-frequency noise we coaveraged 75 consecutive scans and sent them through a digital low-pass Butterworth filter. The largest source of optical noise in the system was etalon fringes that originated in the White cell and optics.

Spectral shifting of the spectrum can occur as the result of slight temperature variations of the heat sink for the laser. To counteract this shifting effect we used the H_2O absorption peak at 1912.5 cm^{-1} shown in Fig. 3 as a spectral reference to line up each spectrum before coaveraging to reduce smear and improve detection sensitivities. A custom software program was used to control the external functions of the lock-in amplifier, function generators, and current driver by use of IEEE-488.2 general-purpose interface bus communications. The software also performed the coaveraging, filtering, and spectral analysis algorithms for determining concentrations based on breath eNO/eCO_2 ratios that we discuss later in this paper. A second-harmonic spectrum of human breath containing peaks for NO, CO_2 , H_2O , and associated HITRAN absorption line strengths is shown in Fig. 3.

Second-harmonic spectra contain absorption magnitudes that are directly proportional to concentrations of the associated molecular species. A calibration curve of the instrument was generated by use of the gas dilution system depicted in Fig. 4, which is designed for diluting a $10 \text{ ppm} \pm 2\%$ NO gas

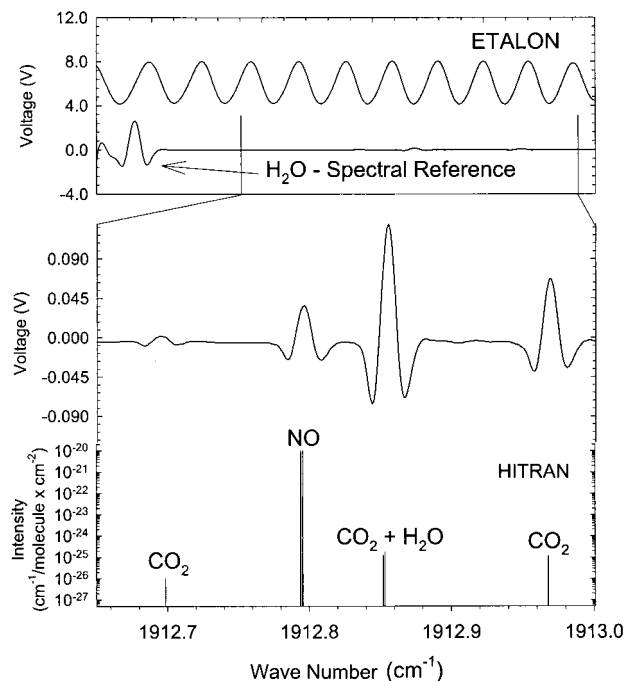


Fig. 3. Second-harmonic spectrum of exhaled alveolar-enriched breath measured at 1912.5 – 1913.0 cm^{-1} . Top, the entire spectrum with a strong H_2O absorption feature at 1912.55 cm^{-1} along with the etalon fringe (free spectral range of the etalon, 0.048 cm^{-1}). Bottom, the absorption features of NO, CO_2 , and H_2O are highlighted. The NO line of interest is at 1912.79 cm^{-1} , and the CO_2 line of interest is located at 1912.96 cm^{-1} .

standard (Airgas, Mobile, Ala.) with purified N_2 . Mass-flow controllers located at the inlet to the White cell were used to mix various flows of NO with N_2 to achieve continuous flow concentrations from 10 ppb to 20 ppb. To quantify concentrations we collected a reference spectrum at a known concentration of 50 ppb. The absorption magnitude of a 50-ppb NO reference spectrum was then compared with subsequent absorptions of NO at concentrations as diluted as 20 ppb by use of a least-squares fitting routine described in Ref. 30. The least-squares fitting routine returned the average absorption magnitude over the entire spectral feature including both negative lobes,

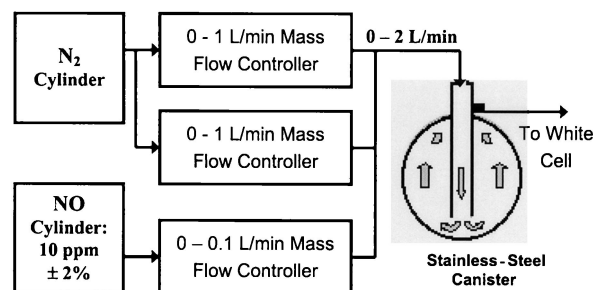


Fig. 4. Schematic of the gas dilution system capable of producing calibrated NO concentrations of 20 ppb–10 ppm by dilution of a 10-ppm NO gas standard with purified N_2 . Continuous flow through the stainless-steel canister ensured steady-state homogeneous mixing of the NO and N_2 .

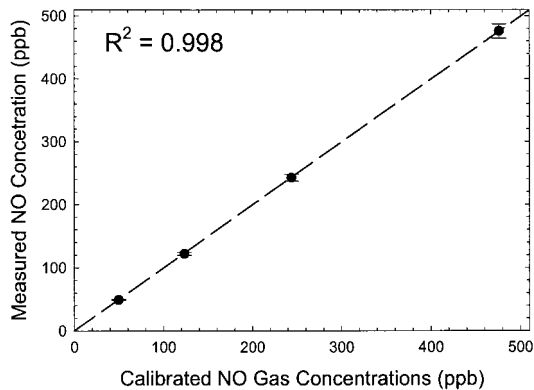


Fig. 5. Gas calibration curve obtained by measuring concentrations of NO produced with the gas dilution system. The curve shows a strong linear relationship ($R^2 = 0.998$) between the diluted NO gas samples and the measured absorption intensities. The error bars represent the standard deviation of 200 consecutive measured NO data points for each concentration.

which is more accurate than just measuring the peak of the absorption feature. Details of the least-squares fitting routine are described in Section 5. The calibration curve showing diluted NO gas standard calibrations versus measured NO is shown in Fig. 5. The error bars for the points in Fig. 5 represent the standard deviation over 200 consecutive data points measured at each calibration concentration. The line shapes at several concentrations are shown in Fig. 6. Measured NO absorption magnitudes have a strong linear relationship ($R^2 = 0.998$) with calibrated NO concentrations. The minimum detection limit for a 4-s integration time (75 co-adds) was determined to be 1.5 ppb, based upon the V_{rms} noise in the baseline of the second-harmonic spectrum. Further improvement of this figure of merit is possible with faster electronics to collect more spectra in a given time.

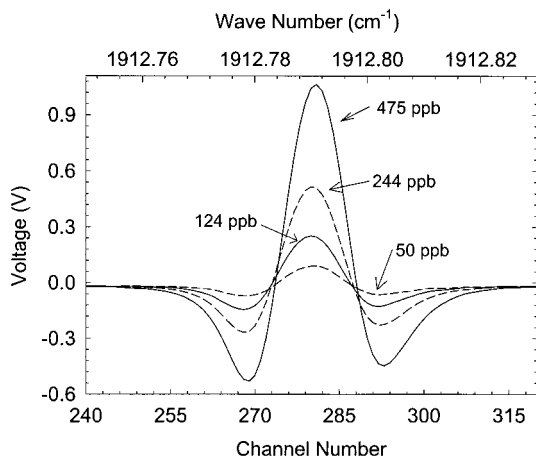


Fig. 6. Measured second-harmonic absorption features of NO (1912.79 cm^{-1}) for concentrations of 50, 124, 244, and 475 ppb. Each spectrum was obtained in a 4-s integration time (75 co-averages) at a cell pressure of 13 Torr.

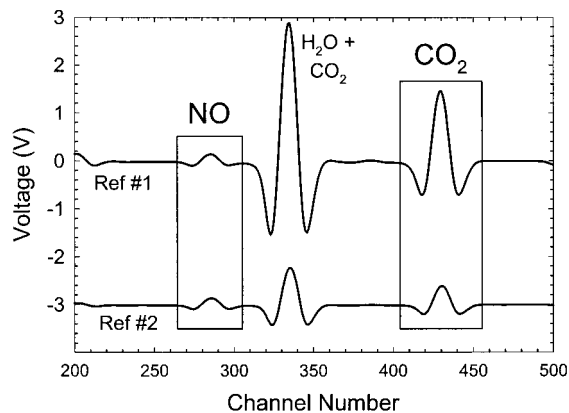


Fig. 7. Two reference spectra (Ref #1 and Ref #2) at various unknown concentrations of NO and CO_2 . The reference spectra are compared with measured signals over the entire absorption profiles for NO and CO_2 , as shown by rectangular windows.

5. Breath Analysis

Breath measurements were performed at a pressure of 13 Torr to reduce line broadening and interference among NO, CO_2 , and H_2O . A mechanical vacuum pump induced flow through the gas cell that was maintained at a constant rate of 2 L/min by the flow controllers. This rate of gas suction was comfortable for patients exhaling into the system over a period of 20 s or less. The breath-collection device (Quintron, Milwaukee, Wisc.) was designed to collect single exhalations and consisted of a T-shaped piece connected to a disposable mouthpiece, a 500-mL discard bag, and a 0.635-cm (0.2 in.) diameter Teflon tubing to direct breath through the flow controllers and into the White cell. The discard bag accepted the first 500 mL of breath at little to no breathing resistance. This headspace breath contains a high concentration of NO that originates from the nasal cavity. The remaining exhaled air entered the Teflon tubing at a constant rate of 2 L/min. Volunteers were instructed to exhale a single breath with force, which assisted in closing the velopharyngeal aperture, limiting the entry of nasal NO via the posterior nasopharynx.⁶ A one-way flutter valve located at the entrance to the discard bag prevented headspace breath from reentering the breath-collection system, and the discard bag was manually emptied after each exhalation. All breath measurements given in this paper are single breath exhalations for 20 s unless otherwise stated. Institutional Review Board approval was granted from the University of Oklahoma for human subjects research, and each participant signed an informed consent form before donating breath.

The magnitude of absorption that was due to breath eNO and e CO_2 was determined by use of a least-squares fitting routine, which uses a reference spectrum to analyze measured spectra during breath testing. Two reference spectra, denoted #1 and #2, at unknown but different concentrations of NO and CO_2 are shown in Fig. 7. The rectangular windows

that encompass the NO and CO₂ absorption features define the windows that we used to compare the reference spectra with the measured spectra; they include both negative lobes and the absorption peak. To characterize the relationship between the NO and CO₂ absorption profiles within each reference we subtracted background spectra from each reference spectrum to eliminate any baseline offset. Next, we determined the peak absorption voltages to obtain a voltage ratio ($V_{\text{NO}}/V_{\text{CO}_2}$).

During breath donations, measured spectra containing the absorption features for eNO and eCO₂ were compared to either reference spectrum #1 or reference spectrum #2 by the least-squares fitting routine. The measured absorption-line features contained in the set window for the sample (Y) and the reference (X) have a linear relationship of the form $Y_j = a + bX_j$. Here X and Y are the measured voltage amplitudes within a window containing the entire absorption feature including the negative lobes and some baseline on either side. The amplitude scaling factor, b , represents the absorption magnitude determined with the least-squares method shown in Eq. (1) below. Coefficient a represents baseline offset and is ignored. Subscript j in this equation represents the position of the channel number in acquired spectra as shown in Fig. 6:

$$b = \frac{\left(\sum Y_j\right)\left(\sum X_j\right) - N\left(\sum X_j Y_j\right)}{\left(\sum X_j\right)^2 - N\left(\sum X_j^2\right)}. \quad (1)$$

Example eNO and eCO₂ absorption magnitude arrays over time obtained for 20-s breath donations from a nonasthmatic and an asthmatic volunteer are shown in Fig. 8. The end-tidal (or maximum) values in Fig. 8 occur after the end of the exhalation period because there are short delays caused by gas exchange and software processing overhead. We performed and averaged 5 s of NO and CO₂ before-exhalation measurements to determine their absorption magnitudes in the ambient air. We determine the absorption magnitude for eCO₂, b_{eCO_2} , by taking the end-tidal value in the exhalation trend array $[b_{\text{eCO}_2}]_i$. Subscript i in the exhalation trend array denotes absorption magnitude data points collected over the breath-analysis period. The maximum b_{eCO_2} value is used to verify correct breath donation; this works as a good verification because eCO₂ concentrations are always greater than CO₂ concentrations in ambient air. The absorption value in the $[b_{\text{eNO}}]_i$ array measured during the exhalation period that most deviates from the established baseline absorption magnitude for NO in the ambient is used to determine b_{eNO} . For determining b_{eNO} it is not proper to use only the maximum value in $[b_{\text{eNO}}]_i$ because it is possible to have larger NO concentrations in ambient air than in exhaled breath. Once b_{eNO} and b_{eCO_2} have been determined, we use the following equation to describe the overall absorption

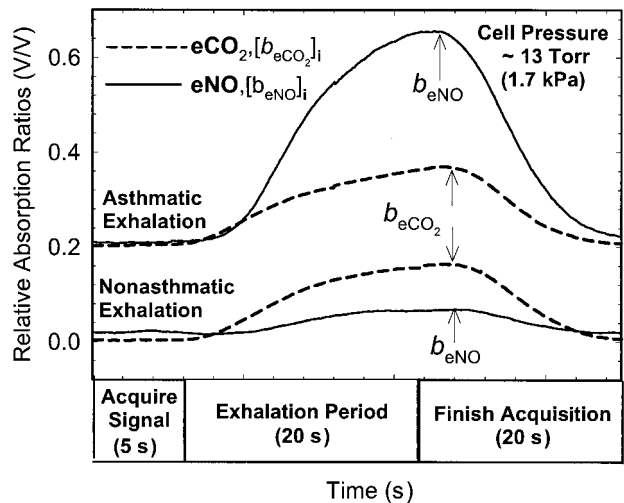


Fig. 8. Exhalation trends of eNO and eCO₂ measured from an asthmatic participant and from a nonasthmatic participant over a 20-s exhalation. The asthmatic participant had end-tidal eNO absorption magnitudes (b_{eNO}) that were 3× larger than the nonasthmatic, and both had similar end-tidal eCO₂ absorption magnitudes (b_{eCO_2}).

ratio, $A_{\text{eNO}}/A_{\text{eCO}_2}$, that relates the measured absorption magnitudes of analyzed breath samples to the voltage magnitudes of the reference spectra:

$$\frac{A_{\text{eNO}}}{A_{\text{eCO}_2}} = \frac{b_{\text{eNO}}}{b_{\text{eCO}_2}} \times \frac{V_{\text{NO}}}{V_{\text{CO}_2}}. \quad (2)$$

Utilizing known standard line strengths $[S(v)]$ and pressure broadening coefficients (g) found in the HITRAN database, we can use the following equation to relate the concentrations of eNO and eCO₂ in breath, where C_{eNO} and C_{eCO_2} represent concentrations of eNO and eCO₂, respectively:

$$C_{\text{eNO}} = \left(\frac{A_{\text{eNO}}}{A_{\text{eCO}_2}}\right) \left(\frac{g_{\text{NO}}}{g_{\text{CO}_2}}\right) \left[\frac{S(v)_{\text{CO}_2}}{S(v)_{\text{NO}}}\right] \times C_{\text{eCO}_2}. \quad (3)$$

We derived Eq. (3) by using Beer's law and the fact that second-harmonic spectra produce absorption magnitudes that have an approximately linear relationship to the concentration of the absorbing gas species. In Eq. (3) it is assumed that laser power is equivalent across both the NO and the CO₂ absorption lines. To solve for C_{eNO} we assumed that eCO₂ concentrations are 4%, which is the typical value for exhaled C_{eCO_2} in human breath.³¹ Equation (3) is vulnerable to error if the actual value of C_{eCO_2} from an individual deviates significantly from 4%. Slight variations ($\pm 10\%$) in actual C_{eCO_2} , however, do not significantly affect the interpreted results because it is not critically clinically important at this time to obtain high-precision eNO concentrations. A 10% variation in eCO₂ concentration would give a typical error of ± 2 ppb in the calculated eNO concentration, which is much smaller than the difference between eNO concentration ranges for asthmatics (30–80 ppb) and nonasthmatics (5–20 ppb).¹

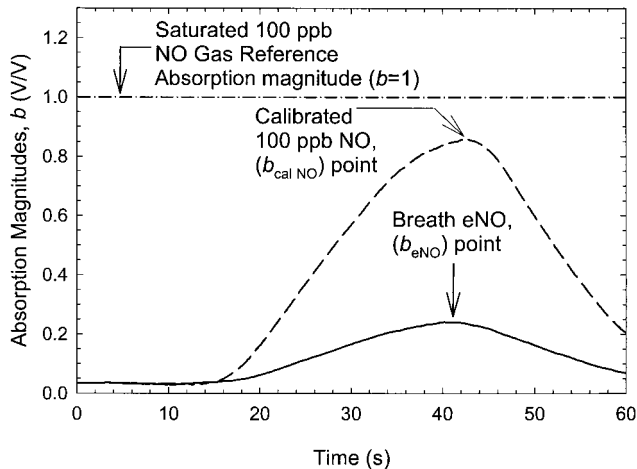


Fig. 9. Absorption magnitude of NO versus time for 100-ppb NO gas flowed through the cell for 20 s and for a volunteer's breath for a 20-s exhalation. The two trends were compared with the calibrated eNO concentrations by use of Eq. (4). An absorption magnitude of $b = 1$ corresponds to the White cell's being completely saturated with 100-ppb NO gas.

6. Results of eNO Breath Measurements

Results of testing five individuals (four nonasthmatics and one asthmatic) with reference spectra #1 and #2 over a period of 10 days are presented. Calibrated eNO levels are compared with calculated eNO concentrations by use of Eq. (3). Also given are the results of studying different breath-testing parameters including various exhalation times, White cell pressures, and ambient NO levels.

For reference spectrum #1, each participant gave three breaths, and the eNO results calculated with Eq. (3) were averaged over the three breaths. The same procedure was repeated with reference spectrum #2. To perform calibration measurements for each participant we flowed a diluted NO standard of 100 ppb through the White cell for 20 s, just as if a participant were exhaling. Figure 9 shows an example concentration trend for calibrated NO flowing through the gas cell. The 100-ppb NO signal over the 20-s period was compared with a reference spectrum collected while the White cell was saturated with 100 ppb of NO and the associated average absorption magnitude (b) was ~ 1.0 , as indicated in Fig. 9. The 100-ppb NO sample flow for 20 s does not completely saturate the White cell volume of 16 L at a gas exchange rate of 2 L/min, and a small software time constant that is due to data computational overhead does not allow $b_{\text{cal eNO}}$ to completely reach 1.0. Immediately following analysis of the 100-ppb NO calibration gas the volunteer exhaled into the system, and the absorption magnitude for b_{eNO} was then compared with the 20-s 100-ppb calibration NO absorption magnitude, $b_{\text{cal NO}}$. The calibrated eNO concentration, $C_{\text{cal eNO}}$, was calculated as follows:

$$C_{\text{cal eNO}} = \left(\frac{b_{\text{eNO}}}{b_{\text{cal NO}}} \right) \times (100 \text{ ppb Reference NO}). \quad (4)$$

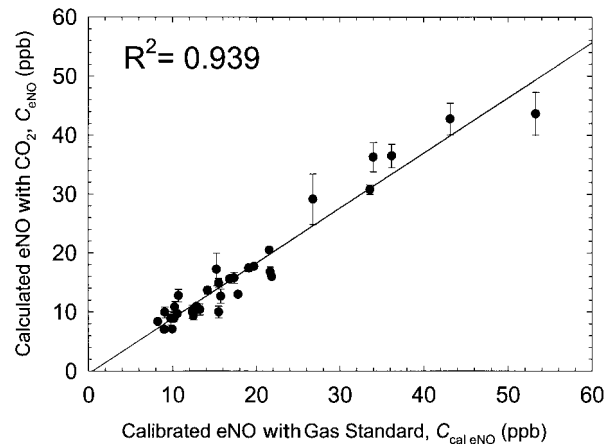


Fig. 10. Plot of calibrated eNO breath measurements quantified with a 50-ppb NO gas standard versus eNO concentrations calculated with the eCO_2 absorption magnitudes and Eq. (3). The linear relationship ($R^2 = 0.939$) between calibrated and calculated eNO concentrations validates the use of eCO_2 as an internal calibration gas. Each point represents the mean of three consecutive measurements of eNO calculated from each volunteer, and the error bars represent the standard deviation.

Three sequential calibrated eNO breath measurements were performed and averaged to yield the calibrated eNO concentration, $C_{\text{cal eNO}}$. It should be noted that a 16-L cell volume is suitable when one is discarding headspace, but smaller cell volumes are more desirable for rapid gas exchange rates and improved temporal resolution.

Each of the five participants donated nine breaths daily over the period of ten working days (three breaths for Ref. #1, three breaths for Ref. #2, and three breaths for calibration). The relationship between calibrated eNO results and calculated eNO results for references #1 and #2 over the ten-day period are shown by error bars in Fig. 10. There was a good linear relationship ($R^2 = 0.939$) between the two methods, showing that Eq. (3) including a 4% value for eCO_2 concentrations permitted accurate eNO measurements over the 2-week testing period.

Adults found the 20-s exhalation time comfortable for a constant 2-L/min flow rate. The young, the elderly, or the ill, however, may find a 20-s exhalation period too long. Figure 11 shows the results of an adult participant's exhaling for periods of 15, 10, and 5 s, which would simulate breath collection from a child or from an adult with limited lung function. The longer the exhalation times, the stronger the measured signals, because there will be more NO and CO_2 molecules occupying the White cell. However, the eNO and eCO_2 ratios together help to account for variations in exhalation times, and they resulted in little variation in calculated eNO concentrations when Eq. (3) was used: the concentrations were 10.6 ± 0.75 , 11.7 ± 0.25 , and 11.6 ± 0.57 ppb for 5, 10, and 15 s, respectively.

Figure 12 shows eCO_2 trends from an individual exhaling at sample cell pressures ranging from 13 to 33 Torr. As the pressure increases, the volume in-

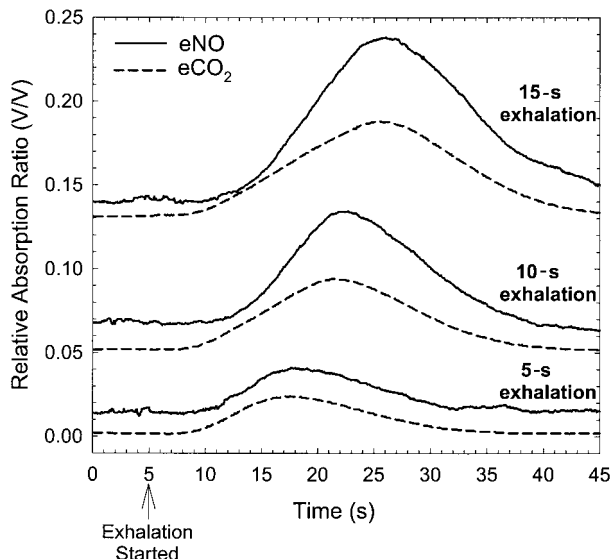


Fig. 11. Comparison of breath measurements at exhalation times of 5, 10, and 15 s. eNO concentrations calculated with Eq. (3) for the three exhalations were in good agreement. A 5-s exhalation time would simulate an exhalation time for a young child or an elderly or a very ill person.

creases, and the trends have a less apparent plateau because breath is not filling as much of the White cell volume. Figure 13 shows the calculated eNO results versus pressure. Varying the exhalation times and the cell pressures does not appear to affect calculated eNO results significantly.

During the early morning and evening rush hours, NO levels in ambient air have been observed to be as high as 200 ppb, mainly as a result of automobile exhaust.³² To test the effect of elevated NO levels on measured eNO values, a volunteer donated breath in the morning when ambient NO levels were high, above 20 ppb, and again in the midafternoon when

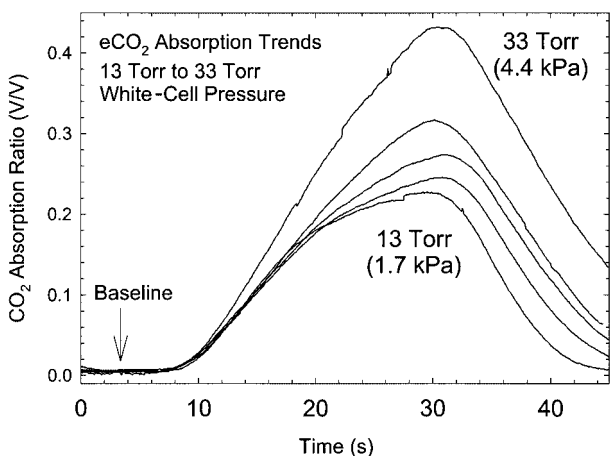


Fig. 12. Exhalation trends for eCO₂ at various pressures from 13 Torr (1.7 kPa) to 33 Torr (4.4 kPa). At higher pressures, gas exchange rates increase, resulting in larger times required for eCO₂ to escape the cell. The peak eCO₂ absorption magnitudes in each trend at lower pressures decrease because there are fewer CO₂ molecules occupying the White cell.

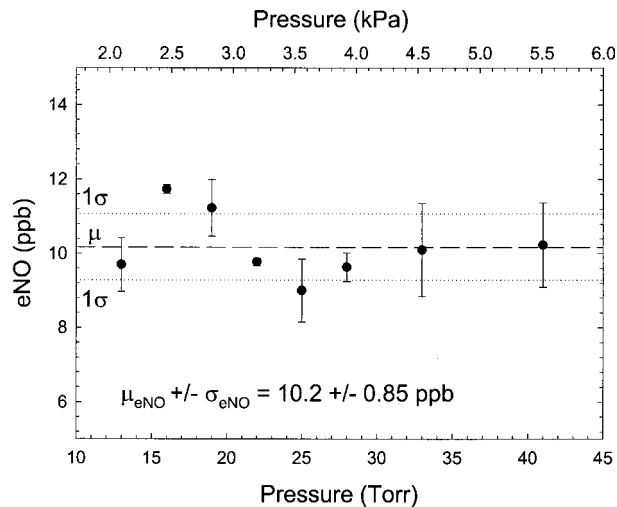


Fig. 13. eNO concentrations calculated with Eq. (3) at various pressures from 13 to 40 Torr along with eNO concentration mean, μ_{eNO} , and the standard deviation, σ_{eNO} . Varying the White cell pressure did not significantly affect the measured eNO concentrations. Each point represents the mean of three consecutive measurements of calculated eNO from each volunteer, and the error bars represent the standard deviation.

ambient levels were below 5 ppb. Figure 14 shows the eNO and eCO₂ trends for both breath donations from the same volunteer. When NO concentrations in ambient air are larger than eNO in breath, breath eNO displaces ambient NO in the cell, and the total concentration of NO in the cell goes down. Lower eNO concentrations than ambient NO concentrations suggest that inhaled NO from the ambient air is rapidly absorbed by airway tissues and is not subsequently exhaled. Recent *in vivo* measurements of NO and its chemical reaction products in human airways showed that NO rapidly consumes reactive oxidative species, producing few reactive intermediate compounds such as ONOO— and ONOOH.³³ This process leads to the accumulation of the innocuous product NO₃—. We suggest that high eNO levels in the breath of an asthma sufferer may actually be associated with a protective mechanism in which production of endogenous NO reduces the concentration of more-damaging reactive oxidative species that are also produced in the airways of individuals with asthma. The observation of exhaled NO concentrations that are lower than ambient levels shows that ambient (exogenous) NO is also rapidly consumed by airway tissues. It is not clear whether such consumption in the lungs of healthy or asthmatic individuals is beneficial.

Elevated NO in ambient air can act as a source of interference when one is using chemiluminescence; however, the breath-collection method described in this paper coupled with a mid-IR TLAS system provided for repeatable eNO measurements in spite of high or low ambient NO concentrations. Eliminating ambient NO concentrations as a factor influencing reproducibility allows the instrument to be

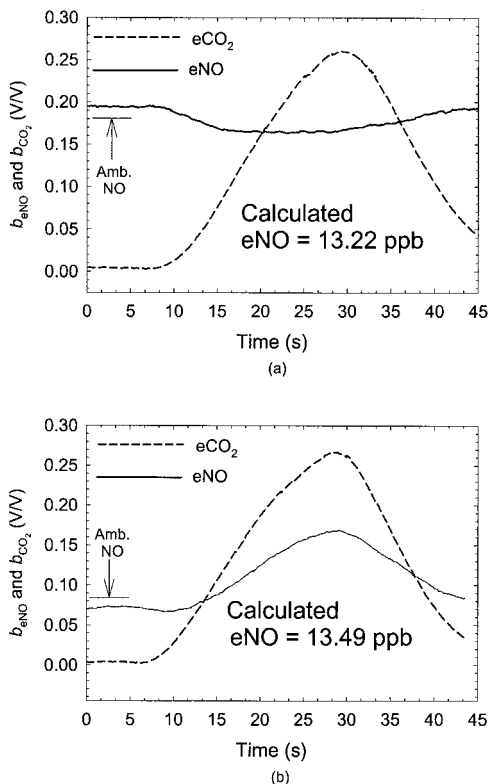


Fig. 14. (a) Breath eNO and eCO₂ exhalation trends measured from a nonasthmatic individual at 9:00 AM when the ambient (Amb.) NO was greater than eNO. (b) eNO and eCO₂ exhalation trends measured at 2:00 PM when ambient NO levels were less than eNO concentrations. Ambient NO concentrations do not significantly affect calculated eNO concentrations when Eq. (3) is used.

operated in environments where air pollution effects are significant.

7. Clinical Applications of eNO Breath Analysis

An example of how this technology may be clinically useful can be seen from Fig. 15. The lower plot shows eNO concentrations for a healthy volunteer, indicating that eNO is below 20 ppb in the absence of disease. The upper plot shows eNO concentrations for a 42-year-old white male who initially did not carry a diagnosis of asthma. He did have a history of severe seasonal allergies, including allergic rhinitis. The patient did experience intermittent chest heaviness, though he denied more-obvious symptoms of the disease. His initial spirometry was normal; however, subsequent methacholine challenge testing was positive, indicating hyperreactive airways and a likely diagnosis of asthma. The patient's eNO was found to be elevated (>40 ppb), and subsequently a trial of inhaled glucocorticoids was undertaken. As illustrated in Fig. 15, by the 9-day mark the patient's eNO had fallen dramatically and was in the normal range of <20 ppb. Despite his initial lack of symptoms, the patient subjectively felt much better with the inhaled glucocorticoids.

Methacholine is a medication that will induce air-

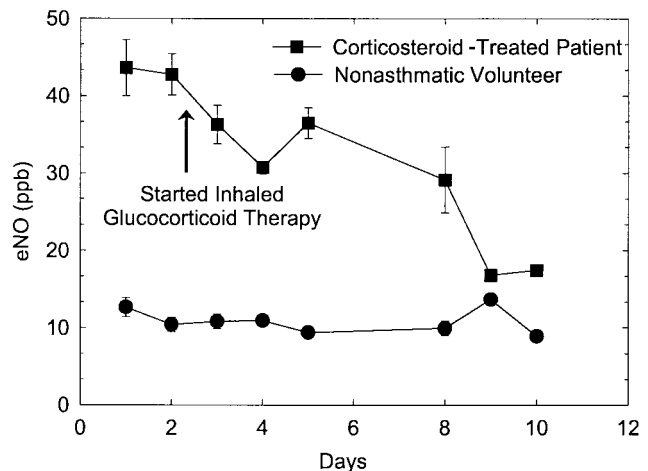


Fig. 15. Daily measurements of eNO with Eq. (3) over a period of 10 days. The eNO concentrations from the nonasthmatic volunteer remained in the normal range from 10 to 15 ppb over the 10-day measurement period. Note the reduction in eNO concentrations for the asthmatic volunteer between day 2 and day 3 after inhaled glucocorticoid therapy was begun. A reduction in eNO confirms the anti-inflammatory action of the glucocorticoid medication.

way obstruction only in the presence of hyperreactive airways. A positive test is indicated by a 20% fall in the measured baseline forced expired volume in 1 s (conventionally abbreviated FEV₁). This has been the so-called gold standard for establishing the diagnosis of asthma, a disease that can be quite variable in its presentation. Despite its utility, the methacholine challenge test is time consuming (~1 h), rather cumbersome, expensive to perform, and potentially risky because a bronchoconstrictive drug is administered. It certainly is not suitable for routine monitoring of the asthmatic patient. Unlike the methacholine test, the eNO test is fast, easy to perform, and economical and presents essentially no risk to the patient. It provides an assessment of underlying airway inflammation, which is a chronic condition in asthma patients. Other asthma diagnostic tests such as spirometry and peak flow measurement evaluate the airway constrictive component of the disease, a typically acute condition that may not be present during a clinical evaluation. The IV-VI laser-equipped TLAS system described here and its ability to determine eNO concentrations in real time with ppb sensitivities may thus prove to be a valuable clinical tool in the near future for the diagnosis and monitoring of asthma.

8. Conclusion

We have presented results of using a mid-IR tunable-laser absorption spectroscopy system equipped with a IV-VI diode laser to measure exhaled nitric oxide. Experimentally determined minimum detection limits for NO were estimated to be 1.5 ppb for a 4-s integration time, performance characteristics that facilitated the demonstration of real-time measurement of eNO. Results illustrate the flexibility of the

measurement technique and its suitability for use in clinical applications. The need for liquid N₂ was eliminated by the inclusion of a closed-cycle cryogenic refrigerator to cool both the laser and the detector in the TLAS system. Internal calibration was accomplished by use of exhaled CO₂ absorption magnitudes measured simultaneously with eNO, eliminating the need for calibration gases. The effects of varying sample cell pressures, exhalation times, and ambient NO concentrations were studied and had little effect on calculated eNO levels obtained with the algorithm described in this paper. We used the TLAS system to perform daily eNO measurements, and our results demonstrated the capability of this technique to monitor the effectiveness of anti-inflammatory treatments. By addressing the problems associated with chemiluminescence eNO measurements, TLAS has been shown to be a capable and user-friendly tool for next-generation eNO analysis in clinical settings. The simplified breath-collection procedure described for the TLAS system should make the eNO measurement technique suitable for pediatric patients under the age of 8 years. Future research should include studies of pediatric patients and include investigation of integrating a low-cost CO₂ sensor to account for the variation of eCO₂ levels in individuals.

References

1. D. H. Yates, "Role of exhaled nitric oxide in asthma," *Immunol. Cell Biol.* **79**, 178–190 (2001).
2. K. Alving, E. Weitzberg, and J. M. Lundberg, "Increased amount of nitric oxide in exhaled air of asthmatics," *Eur. Respir. J.* **6**, 1368–1370 (1993).
3. S. A. Kharitonov and P. J. Barnes, "Clinical aspects of exhaled nitric oxide," *Eur. Respir. J.* **16**, 781–792 (2000).
4. K. J. Haley and J. M. Drazen, "Inflammation and airway function in asthma, what you see is not necessarily what you get," *Am. J. Respir. Crit. Care Med.* **157**, 1–3 (1998).
5. M. Bernareggi and G. Cremona, "Measurement of exhaled nitric oxide in humans and animals," *Pulmonary Pharmacol. Therapeut.* **12**, 331–352 (1999).
6. P. E. Silkoff, "Recommendations for standardized procedures for the online and offline measurement of exhaled lower respiratory nitric oxide and nasal nitric oxide in adults and children—1999," *Am. J. Respir. Crit. Care Med.* **160**, 2104–2117 (1999).
7. S. Kharitonov, K. Alving, and P. J. Barnes, "Exhaled and nasal nitric oxide measurements: recommendations (ERS Task Force Report)," *Eur. Respir. J.* **10**, 1683–1693 (1997).
8. P. E. Silkoff, P. A. McLean, A. S. Slutsky, H. G. Furlott, E. Hoffstein, S. Wkita, K. R. Chapman, J. P. Szalai, and N. Zamel, "Marked flow-dependence of exhaled nitric oxide using a new technique to exclude nasal nitric oxide," *Am. J. Respir. Crit. Care Med.* **155**, 260–267 (1997).
9. N. Binding, W. Muller, and P. A. Czeschinski, "NO chemiluminescence in exhaled air: interference of compounds from endogenous and exogenous sources," *Eur. Respir. J.* **6**, 499–503 (2000).
10. K. Namjou, S. Cai, E. A. Whittaker, J. Faist, C. Gmachl, F. Capasso, D. L. Sivco, and A. Y. Cho, "Sensitive absorption spectroscopy with a room-temperature distributed-feedback quantum-cascade laser," *Opt. Lett.* **23**, 219–222 (1998).
11. M. Beck, D. Hofstetter, T. Allen, J. Faist, U. Oesterle, M. Illegems, E. Gini, and H. Melchior, "Continuous wave operation of a mid-infrared semiconductor laser at room-temperature," *Science* **295**, 301–305 (2002).
12. L. Konstantin, A. I. Nadezhdinskii, and I. A. Adamouskaya, "Human breath trace gas content study by tunable diode laser spectroscopy technique," *Infrared Phys. Technol.* **37**, 181–192 (1996).
13. K. Namjou, P. J. McCann, and W. T. Potter, "Breath testing with a Mid-IR laser spectrometer," in *Application of Tunable Diode and Other Infrared Sources for Atmospheric Studies and Industrial Processing Monitoring II*, A. Fried, ed., Proc. SPIE **3758**, 74–80 (1999).
14. K. R. Lewelling and P. J. McCann, "Finite element modeling predicts possibility of thermoelectrically-cooled lead-salt diode lasers," *IEEE Photon. Technol. Lett.* **9**, 297–299 (1997).
15. H. Z. Wu, X. M. Fang, R. Salas, D. McAlister, and P. J. McCann, "Transfer of PbSe/PbEuSe epilayers grown by MBE on BaF₂-coated Si(111)," *Thin Solid Films* **352**, 277–282 (1999).
16. D. W. McAlister, P. J. McCann, H. Z. Wu, and X. M. Fang, "Fabrication of thin film cleaved cavities using a bonding and cleaving fixture," *IEEE Photon. Technol. Lett.* **12**, 22–24 (2000).
17. P. J. McCann, K. Namjou, and X. M. Fang, "Above-room-temperature continuous wave mid-infrared photoluminescence from PbSe/PbSrSe quantum wells," *Appl. Phys. Lett.* **75**, 3608–3610 (1999).
18. X. M. Fang, K. Namjou, I. Chao, P. J. McCann, N. Dai, and G. Tor, "Molecular beam epitaxy of PbSrSe and PbSe/PbSrSe multiple quantum well structures for use in mid-infrared light emitting devices," *J. Vacuum Sci. Technol.* **18**, 1720–1723 (2000).
19. D. W. McAlister, P. J. McCann, K. Namjou, H. Z. Wu, and X. M. Fang, "Mid-IR photoluminescence from IV–VI layers grown on silicon," *J. Appl. Phys.* **89**, 3514–3516 (2001).
20. F. Zhao, H. Wu, L. Jayasinghe, and Z. Shi, "Above-room-temperature optically pumped 4.12 μm midinfrared vertical-cavity surface-emitting lasers," *Appl. Phys. Lett.* **80**, 1129–1131 (2002).
21. A. A. Kosterev, A. L. Malinovsky, F. K. Tittel, C. Gmachl, F. Capasso, D. L. Sivco, J. N. Baillargeon, A. L. Hutchinson, and A. Y. Cho, "Cavity ringdown spectroscopic detection of nitric oxide with a continuous-wave quantum-cascade laser," *Appl. Opt.* **40**, 5522–5529 (2001).
22. L. Menzel, A. A. Kosterev, R. F. Curl, F. K. Tittel, C. Gmachl, F. Capasso, D. L. Sivco, J. N. Baillargeon, A. L. Hutchinson, A. Y. Cho, and W. Urban, "Spectroscopic detection of biological NO with a quantum cascade laser," *Appl. Phys. B.* **72**, 859–863 (2001).
23. C. Roller, K. Namjou, J. Jeffers, W. Potter, P. J. McCann, and J. Grego, "Simultaneous measurement of NO and CO₂ in human breath using a single IV–VI mid-infrared laser," *Opt. Lett.* **27**, 107–109 (2002).
24. E. V. Stepanov, P. V. Zyrianov, and V. A. Miliaev, "Single-breath NO detection with tunable diode lasers for pulmonary disease diagnosis," in *ALT⁹⁸ Selected Papers on Novel Laser Methods in Medicine and Biology*, G. P. Koz'min, A. M. Prokhorov, and V. I. Pustovoy, eds., Proc. SPIE **3829**, 103–109 (1999).
25. J. Reid, D. T. Cassidy, and R. T. Menzies, "Linewidth measurements of tunable diode lasers using heterodyne and etalon techniques," *Appl. Opt.* **21**, 3961–3965 (1982).
26. E. D. Hinkley and C. Freed, "Direct observation of the Lorentzian line shape as limited by quantum phase noise in a laser above threshold," *Phys. Rev. Lett.* **23**, 277–279 (1969).
27. M. Razeghi, S. Slivken, A. Matlis, A. Rybaltowski, C. Jelen, and J. Diaz, "Low threshold quantum cascade lasers grown by GSMBE," *LEOS Newsletter* **12**(6), 5–7 (1998).
28. A. A. Kosterev, R. F. Curl, F. K. Tittel, C. Gmachl, F. Capasso, D. L. Sivco, J. N. Baillargeon, A. L. Hutchinson, and A. Y. Cho,

- “Effective utilization of quantum-cascade distributed-feedback lasers in absorption spectroscopy,” *Appl. Opt.* **39**, 4425–4430 (2000).
29. L. S. Rothman, C. P. Rinsland, A. Goldman, S. T. Massie, D. P. Edwards, J. M. Flaud, A. Perrin, C. Camy-Peyret, V. Dana, J. Y. Mandin, J. Schroeder, A. McCann, R. R. Gamache, R. B. Wattson, K. Yoshino, K. V. Chance, K. W. Jucks, L. R. Brown, V. Nemtchinov, and P. Varanasi, “The HITRAN molecular spectroscopic database and HAWKS (HITRAN atmospheric workstation): 1996 edition,” *J. Quant. Spectrosc. Radiat. Transfer* **60**, 665–710 (1998).
30. A. Fried, J. R. Drummond, B. Henry, and J. Fox, “Versatile integrated tunable diode laser system for precision: application for ambient measurements of OCS,” *Appl. Opt.* **30**, 1916–1932 (1991).
31. J. J. Carr and J. M. Brown, “The human respiratory system and its measurement,” in *Introduction to Biomedical Equipment Technology*, 3rd ed., C. E. Stewart, ed. (Prentice-Hall, Upper Saddle River, N.J., 1998), Chap. 10.
32. A. Mock, C. Roller, K. Namjou, J. Jeffers, P. J. McCann, and J. Grego, “Real-time ground level atmospheric nitric oxide measurements using a calibrated TLDAS system,” in *Laser Applications to Chemical and Environmental Analysis (LA-CEA)*, Vol. 36 of OSA Trends in Optics and Photonics Series (Optical Society of America, Washington, D.C., 2002), pp. SaC4-1–SaC4-3.
33. R. A. Dweik, S. A. A. Comhair, B. Gaston, F. B. J. M. Thunnissen, C. Farver, M. J. Thomassen, M. Kavuru, J. Hammel, H. M. Abu-Soud, and S. C. Erzurum, “NO chemical events in the human airway during the immediate and late antigen-induced asthmatic response,” *Proc. Natl. Acad. Sci.* **98**(5), 2622–2627 (2001).